

Structure of a three-dimensional nano-powder subjected to repeated fragmentation and sedimentation

This content has been downloaded from IOPscience. Please scroll down to see the full text.

2015 New J. Phys. 17 013024

(<http://iopscience.iop.org/1367-2630/17/1/013024>)

View [the table of contents for this issue](#), or go to the [journal homepage](#) for more

Download details:

IP Address: 131.188.126.204

This content was downloaded on 16/01/2015 at 14:47

Please note that [terms and conditions apply](#).



PAPER

Structure of a three-dimensional nano-powder subjected to repeated fragmentation and sedimentation

OPEN ACCESS

RECEIVED

3 October 2014

ACCEPTED FOR PUBLICATION

1 December 2014

PUBLISHED

15 January 2015

Content from this work
may be used under the
terms of the [Creative
Commons Attribution 3.0
licence](#).

Any further distribution of
this work must maintain
attribution to the author
(s) and the title of the
work, journal citation and
DOI.

Nikola Topic¹, Alexander Weuster², Thorsten Pöschel¹ and Dietrich E Wolf²¹ Institute for Multiscale Simulation, Friedrich-Alexander-Universität at Erlangen-Nürnberg, Nagelsbachstrasse 496, 91052 Erlangen, Germany² Fakultät für Physik, Universität Duisburg-Essen, 47048 Duisburg, GermanyE-mail: thorsten.poeschel@fau.de**Keywords:** granular systems, powders, porous materials, fractals, macroscopic aggregates**Abstract**

We revisit the problem of the structure of a nano-powder subjected to repeated fragmentation and sedimentation, and extend the analysis to the more relevant three-dimensional (3D) case. One important question not addressed previously is how the fractal dimension and dust exponent depend on space dimension. We find that the qualitative behavior of the nano-powder in three dimensions is similar to that in two dimensions. But the fractal dimension changes from 1.6 ± 0.1 in two dimensions to 2.1 ± 0.1 in three dimensions. The scaling relation between the fractal dimension and the dust exponent characterizing the fragment size distribution is the same as in two dimensions. The universality of these exponents is addressed by comparing the results with a much simpler lattice model. Although the different settling kinetics of the fragments leads to different anisotropies, the fractal properties are not affected.

1. Introduction

Films of nanoparticles are used in modern gas sensors, solar cells, and many other nanotechnological applications [1]. Such films can be created by sedimenting particles or agglomerates of particles onto a filter or a substrate. Once created, the sediment might be subjected to various treatments as it is handled further, which will modify its structure. Recently it was discovered in two-dimensional simulations that when a nanopowder is subjected to repeated fragmentations and sedimentations, its structure will become invariant to further fragmentations and sedimentations, and it will develop a fractal substructure [2]. It is expected that the scaling behavior depends on space dimension. In this paper the exponents for a three-dimensional extension of the model are presented. Moreover, to address the universality of the phenomenon, we compare also with a much simpler lattice model.

The analysis of the microstructural evolution in a powder handling process that involves millions of particles and hundreds of repeated sedimentation and fragmentation cycles is computationally very challenging. Therefore the development of efficient algorithms constitutes an important part of this paper.

For the sedimentation of spherical particles, Visscher and Bolsterli [3, 4] designed a very efficient but still sufficiently versatile model: the particles are dropped one after another onto a horizontal plane, each one following the trajectory of steepest descent. When a particle reaches a stable position either on three previously dropped spheres or on the ground, it is considered fixed and cannot move anymore. This particle dynamics has been used to study a variety of systems and their phenomena, such as packing properties of sediments [3, 5, 6], their surface properties [7], segregation by size [8, 9], filtration [10], convective heap formation [11], structure evolution in rotating drums [12–14], and how the structure in a heap and its angle of repose are related to the deposition process [15, 16]. In section 2.1 we present a non-trivial generalization of the Visscher–Bolsterli model to agglomerates in three dimensions.

Fragmentation is assumed to happen at a characteristic length scale ℓ . This is modeled by using a simple cubic mesh to cut the sediment into boxes of volume ℓ^3 , which in general contain several disconnected

fragments. We imagine them to be dispersed, for example in a stirred fluid. When stirring stops, the fragments sediment under gravity, leading to the formation of a new agglomerate. During this process the fragments as well as the growing agglomerate are regarded as rigid. Modeling fragmentation by means of discrete elements is an active area of research [17, 18], and interesting phenomena have been found, such as uniqueness of the exponent of the fragment size distribution in a variety of situations. Two-dimensional packings of such fragments have been investigated in [18].

2. Model description

In this section we introduce two three-dimensional models, first an off-lattice model (OLM) in the spirit of the two-dimensional model proposed in [2, 19], and second a similar lattice model (LM) [20].

2.1. Off-lattice model (OLM)

In the off-lattice model, the fragments are dropped one by one with random orientation, and x - and y -coordinates of the center of mass are uniformly distributed over the area $[0, L) \times [0, L)$. In the x and y directions periodic boundary conditions are used. The fragment must be released at a sufficiently high z -coordinate that it can move downward along the negative z -axis until it touches the bottom or a particle that is part of a previously deposited fragment. Then the freshly dropped fragment follows a trajectory of steepest descent of its center of mass. Motion of an arbitrarily shaped fragment can be very complex. To simulate it in an event-driven, efficient way, rolling is replaced by a rigid rotation of the fragment around the center(s) of the fixed sphere(s) underneath. On its course it may detach, fall down, and continue to roll until it settles in a position, where further descent is no longer possible. There it is fixed and cannot move anymore.

The fragmentation of the nano-powder is simulated by cutting the sediment by a cubic mesh with box length ℓ . A particle is considered to belong to a box if its center lies within. The content of each box in general consists of disjoint fragments that have no contact with one another, each one forming a rigid body. These fragments are then individually rotated into random orientations and dropped at random positions as previously described. The newly created packing of fragments is then fragmented again, then deposited, and so on. In the initial sedimentation step spherical particles are dropped.

2.2. Lattice model (LM)

Here a simple cubic lattice is considered with one axis parallel to the z -direction. Particles are represented by filled cells. Each particle can be in contact with up to six nearest neighbors (in the x -, y -, and z -directions). An agglomerate is cut into disjoint cubical boxes of ℓ^3 cells each, as described for the off-lattice model. By means of the Hoshen–Kopelman algorithm [21], the connected clusters (fragments) are identified for all boxes.

For the sedimentation step, first one of the six possible lattice rotations is applied randomly to every fragment. The rotated fragment is then released at a sufficiently large height at randomly chosen lattice coordinates x and y so that it can move down vertically until the first contact in the z -direction is formed. Note that horizontal contacts do not stop the downward motion in this model (see [22]), in contrast with ballistic deposition [23]. No further settling (which would correspond to the steepest descent relaxation in the off-lattice model) takes place here. Once the fragment has reached its final position, all contacts (including the horizontal ones) are supposed to become rigid so that in the next fragmentation step one does not have to discriminate between older and newer contacts.

In the following, we also present data obtained with the two-dimensional version of this lattice model in order to compare them with the two-dimensional off-lattice model [2]. The agglomerates simulated with the lattice model typically consisted of $N = 2^{26}$ particles. All lengths are given in units of the particle diameter (by definition identical with the lattice constant). The horizontal system size was in general $L_x = 4096$ in 2D and $L_x = L_y = 512$ in 3D, and periodic boundary conditions were applied in the x - and y -directions.

2.3. Off-lattice model without relaxation (OLM-)

The lattice model differs from the off-lattice one in two respects: first, there are only six orientations for a fragment; and second, the steepest descent relaxation is absent. To assess their relative importance we also studied the off-lattice model, where the deposited fragment sticks upon first vertical contact, as in the lattice model. The orientation of the fragment before deposition is chosen arbitrarily, but any relaxation is suppressed.

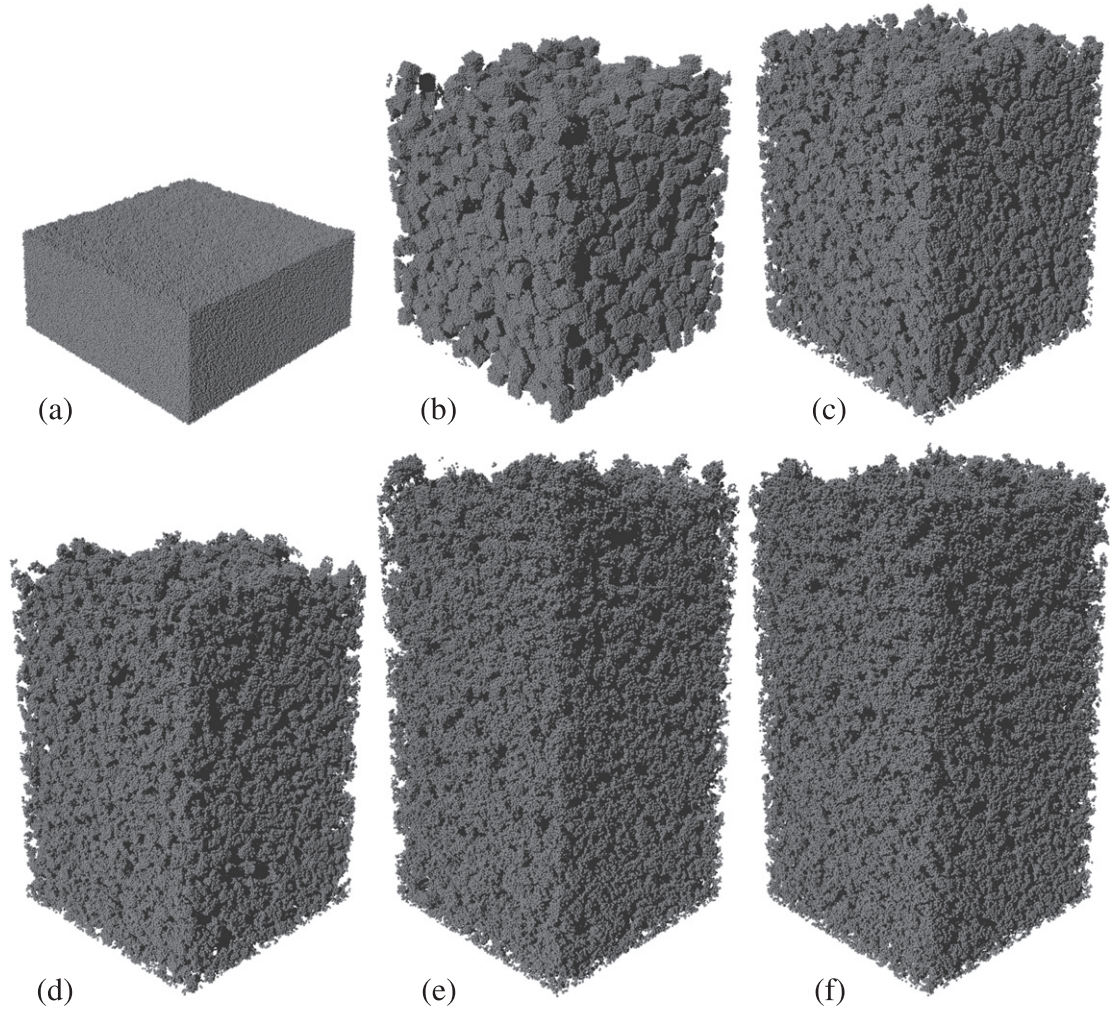


Figure 1. Off-lattice model: evolution of a packing containing $N = 10^6$ particles during repeated sedimentation and fragmentation with $\ell = 8$. The width of the system is $L = 128$. (a) Initial packing of spherical particles. (b) First iteration: sedimented fragments of the initial packing. (c) Second iteration: sedimented fragments of packing (b). (d) Third iteration. Between the 50th iteration (e) and the 100th iteration (f) the structure hardly changes anymore.

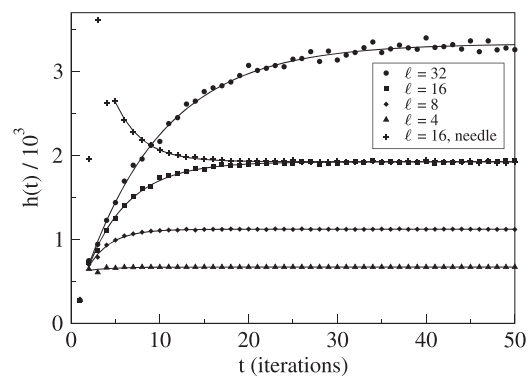


Figure 2. OLM (3D): evolution of the filling height for different fragmentation lengths ℓ . $N = 5 \times 10^6$ and $L = 128$. Heights saturate to ℓ -dependent values $h_\infty(\ell)$. To demonstrate that the steady state is independent of initial conditions, we also considered the case where all particles are part of a single vertical needle at the beginning.

3. Results

In this section we compare the results obtained for five different models: the 2D off-lattice model [2], the 2D lattice model (section 2.2), the 3D off-lattice model (section 2.1), the 3D off-lattice model without relaxation (section 2.3), and the 3D lattice model (section 2.2).

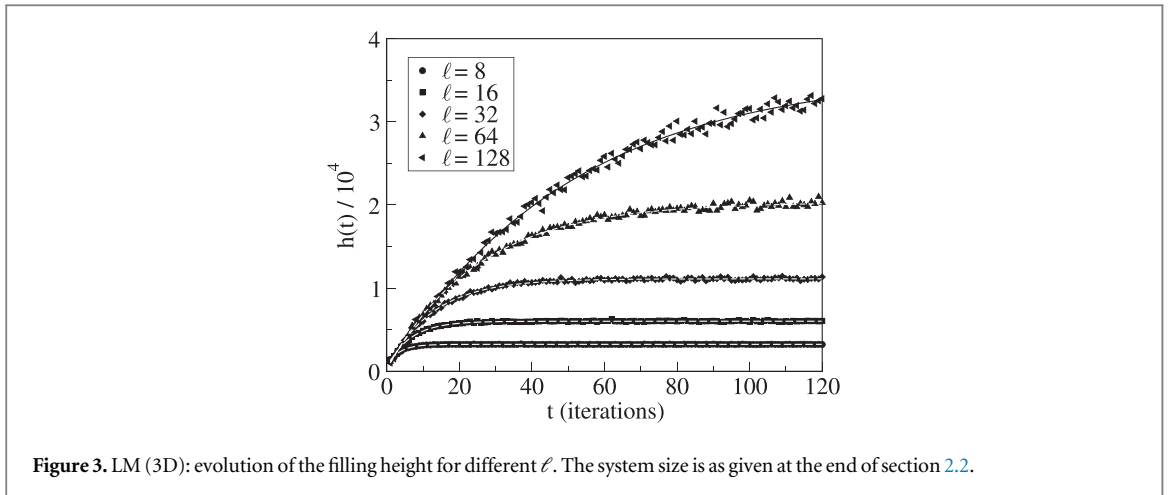


Figure 3. LM (3D): evolution of the filling height for different ℓ . The system size is as given at the end of section 2.2.

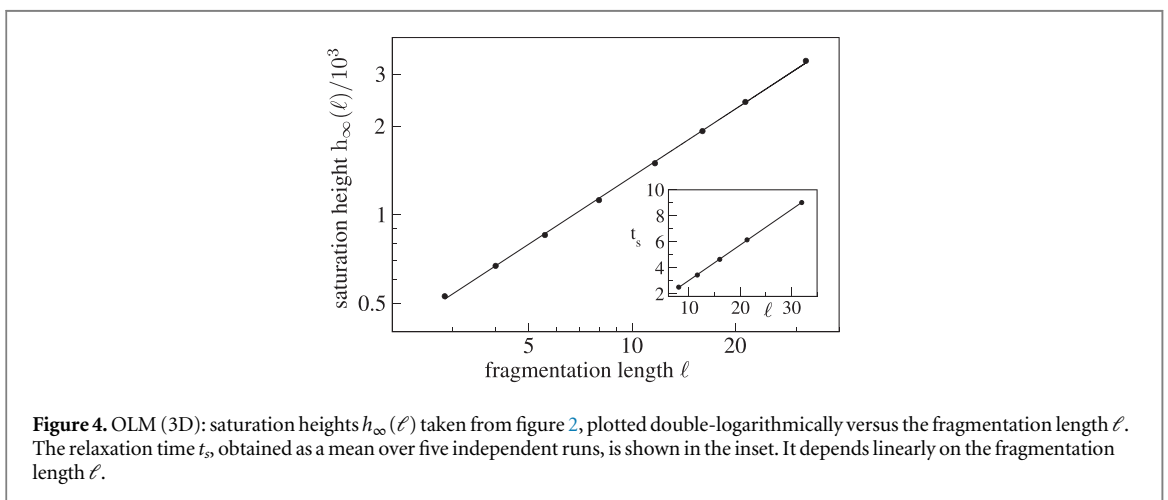


Figure 4. OLM (3D): saturation heights $h_\infty(\ell)$ taken from figure 2, plotted double-logarithmically versus the fragmentation length ℓ . The relaxation time t_s , obtained as a mean over five independent runs, is shown in the inset. It depends linearly on the fragmentation length ℓ .

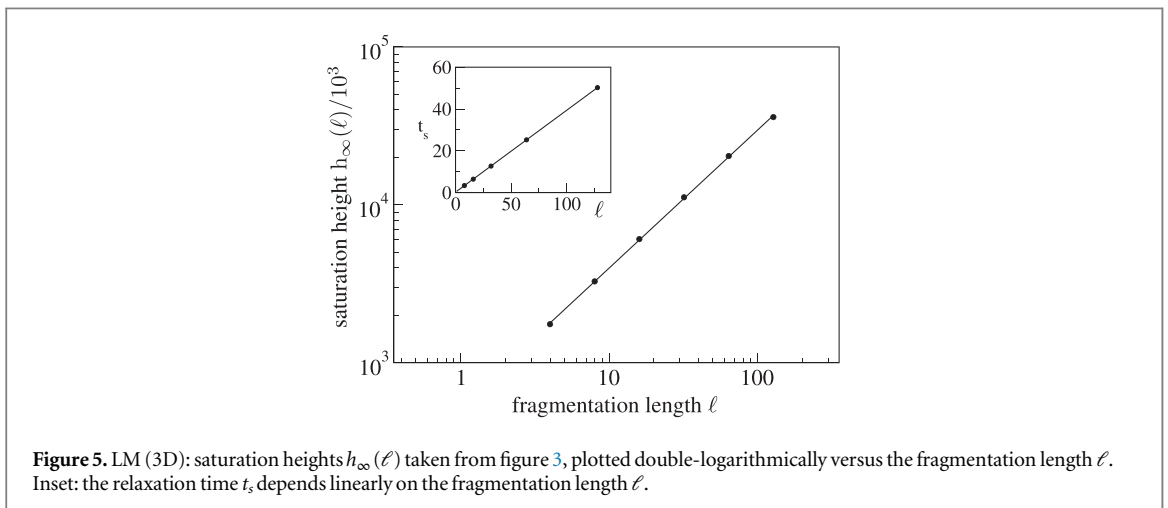


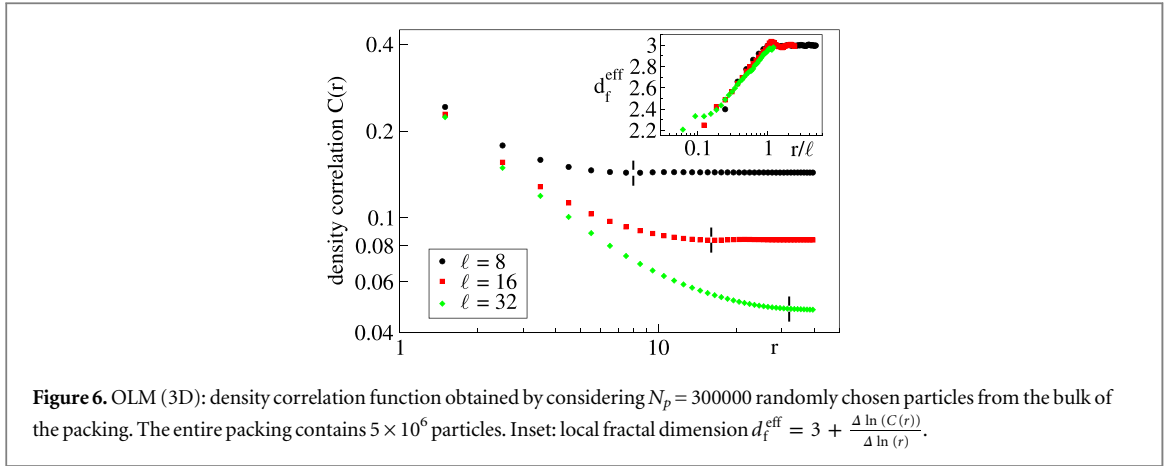
Figure 5. LM (3D): saturation heights $h_\infty(\ell)$ taken from figure 3, plotted double-logarithmically versus the fragmentation length ℓ . Inset: the relaxation time t_s depends linearly on the fragmentation length ℓ .

3.1. Approach of steady state

Figure 1 illustrates the structural evolution of the powder for the off-lattice fragmentation–sedimentation model. The system contains $N = 10^6$ spherical particles with uniformly distributed diameters in the range $[0.9, 1.1]$. The system size and the fragmentation length are $L = 128$ and $\ell = 8$, respectively. The initial sediment, figure 1(a), is a disordered packing with packing fraction of about 0.58. After the first fragmentation and sedimentation, figure 1(b), the structure is dominated by the cube-shaped fragments, which pack into a looser structure than the initial sediment, due to both existing pores inside the cubic fragments and new, much larger pores in between the cubic fragments. After the second iteration, figure 1(c), the fragments have a less well defined shape, and they pack into a looser structure than at the end of the first iteration, evident by the somewhat

Table 1. Exponents for the five models described in the text.

	d_f^h $= d - \alpha$	d_f^c $= d - \gamma$	d_f^m	τ	$d_f^h(2-\tau)$	$d_f^m(2-\tau)$
OLM (2D) (2D off-lattice model [2])	1.67 ± 0.03		1.695 ± 0.005	1.42 ± 0.05	1.03 ± 0.08	1.05 ± 0.08
LM (2D) (2D lattice model, section 2.2)	1.602 ± 0.005	>1.5	1.549 ± 0.007	1.377 ± 0.004	1.00 ± 0.01	0.97 ± 0.01
OLM (3D) (3D off-lattice model, section 2.1)	2.21 ± 0.01	<2.4	2.28 ± 0.03	1.5 ± 0.1	1.12 ± 0.22	1.14 ± 0.23
OLM- (3D) (3D off-lattice without relaxation, section 2.3)	2.128 ± 0.001		1.86 ± 0.04	1.51 ± 0.03	1.04 ± 0.06	0.91 ± 0.06
LM (3D) (3D lattice model, section 2.2)	2.124 ± 0.007	<2.0	1.96 ± 0.03	1.52 ± 0.03	1.02 ± 0.06	0.94 ± 0.06



higher filling height. Another iteration again increases the filling height, figure 1(d). Structures after 50 and 100 iterations have a similar appearance, implying that the structure of the packings has stopped evolving, apart from statistical fluctuations. The fragments blend into a single packing, with no distinct fragment shapes or imprints of mesh structure used for fragmentation. Such a behavior was also observed for the two-dimensional model [2] and for the other models considered in this paper: starting from a random dense packing, repeated fragmentation and sedimentation cycles lead to a monotonous decrease of the solid fraction of the aggregate for all five models. This is reflected by an increasing filling height because the horizontal extent of the systems, $L_x = L_y$, and the number of particles N are fixed.

For two of the models the height evolution is shown in figures 2 and 3. The filling height, determined as twice the center of mass height, saturates for long enough times. The asymptotic values are approached exponentially,

$$h(t, \ell) = h_\infty(\ell) - (h_\infty(\ell) - h_0) e^{-t/t_s(\ell)}, \quad (1)$$

with a relaxation time $t_s(\ell)$, which grows linearly with ℓ in all five models (see insets of figures 4 and 5). In equation (1), h_0 denotes the initial height of the densely packed system, and t the number of cycles. We checked that also the average fragment size and the number of fragments per box reach steady-state values on the same time scale.

The saturation heights averaged over many cycles are plotted double-logarithmically versus ℓ in figures 4 and 5. As for the 2D off-lattice model [2] and the other two models, a power law dependence

$$h_\infty(\ell) \propto \ell^\alpha, \quad (2)$$

is obtained. For the OLM we obtained $\alpha = 0.79 \pm 0.01$, and for the LM $\alpha = 0.876 \pm 0.007$.

In [2] it was argued that the power law dependence of $h_\infty(\ell)$ indicates a fractal substructure up to a linear size ℓ , beyond which the packing becomes homogeneous. The mass density is $\rho(\ell) = M/(L_x L_y h_\infty(\ell))$ with the total mass M . The mass m per box volume $v = \ell^d$ (where d is the dimension of space) is

$$\frac{m}{v} \sim \ell^{d_f^h}. \quad (3)$$

The corresponding fractal dimension $d_f^h = d - \alpha$ is given in the first column of table 1.

3.2. Fractality of steady state

To get direct information about the structure of the packing, we evaluated the density correlation function

$$C(\vec{r}) = \frac{\langle \rho(\vec{r}' + \vec{r}) \rho(\vec{r}') \rangle}{\langle \rho(\vec{r}') \rangle}. \quad (4)$$

The expectation values on the right-hand side are averaged over a large number of steady-state configurations, and over all bulk positions \vec{r}' not too close to the bottom and the surface of the aggregate. In this section we further average over all directions of \vec{r} . The mass density of the individual particles is taken as 1. $C(r)$ becomes equal to the average mass density for large r . If the density correlation function is a power law with exponent $-\gamma$, then the structure is fractal [24], with fractal dimension $d_f^c = d - \gamma$.

The steady-state density correlation function is shown for the 3D off-lattice model in figure 6. In the inset we have plotted the effective fractal dimension

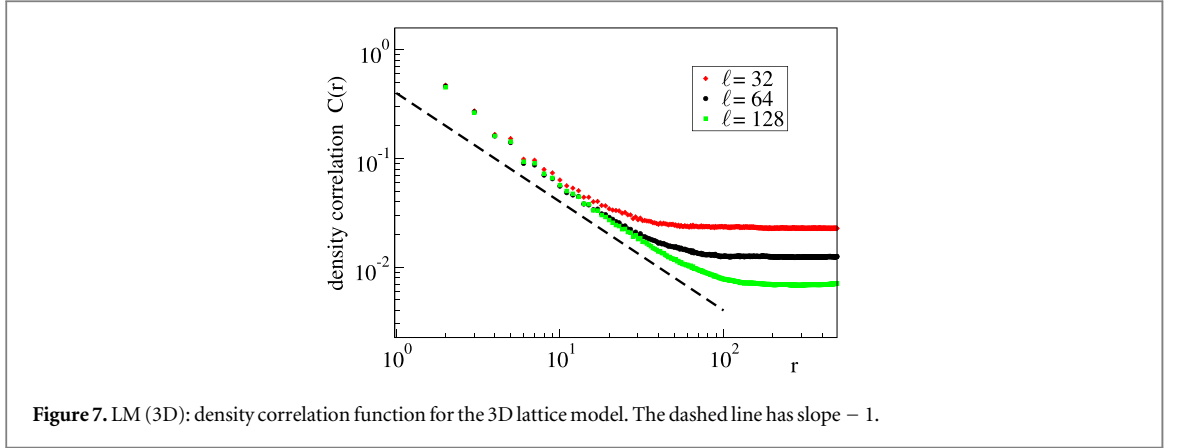


Figure 7. LM (3D): density correlation function for the 3D lattice model. The dashed line has slope -1 .

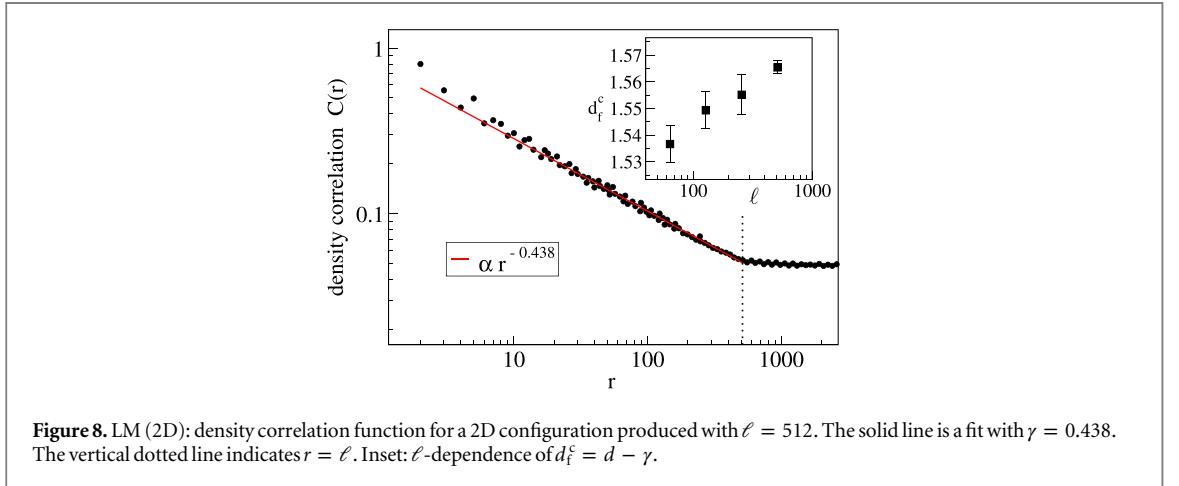


Figure 8. LM (2D): density correlation function for a 2D configuration produced with $\ell = 512$. The solid line is a fit with $\gamma = 0.438$. The vertical dotted line indicates $r = \ell$. Inset: ℓ -dependence of $d_f^c = d - \gamma$.

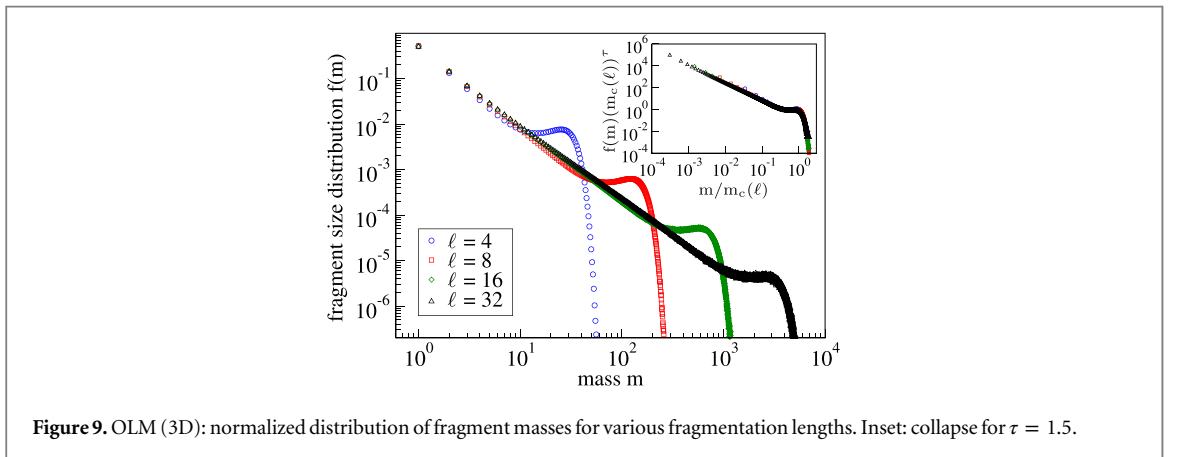
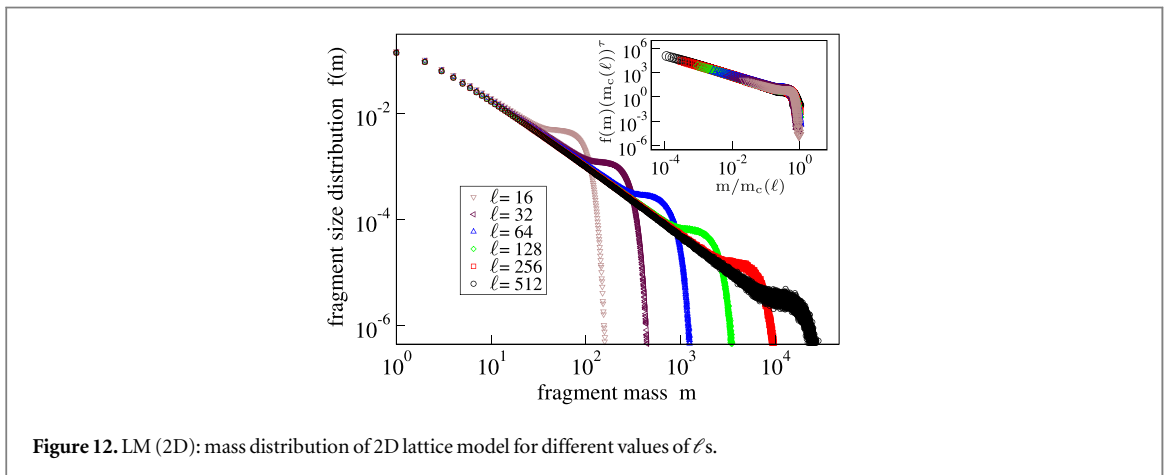
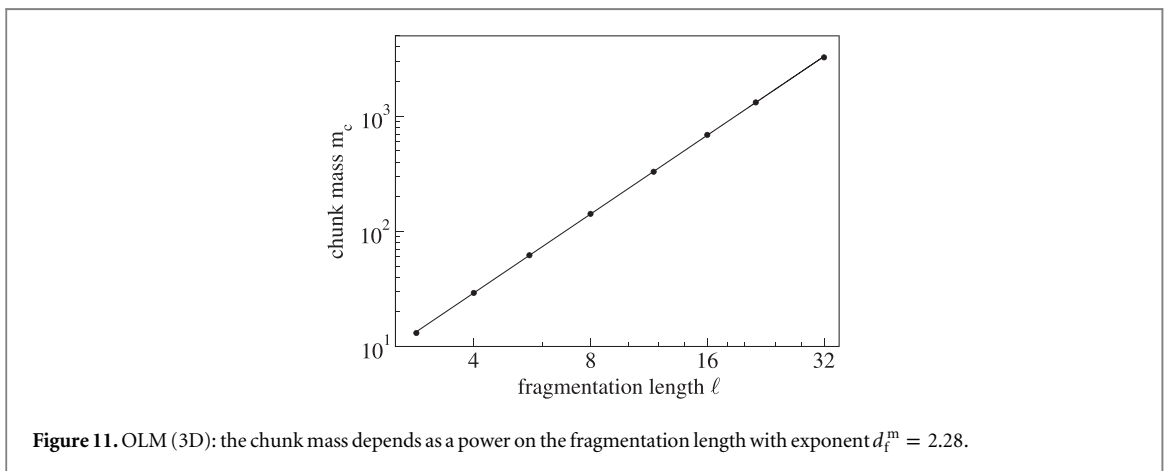
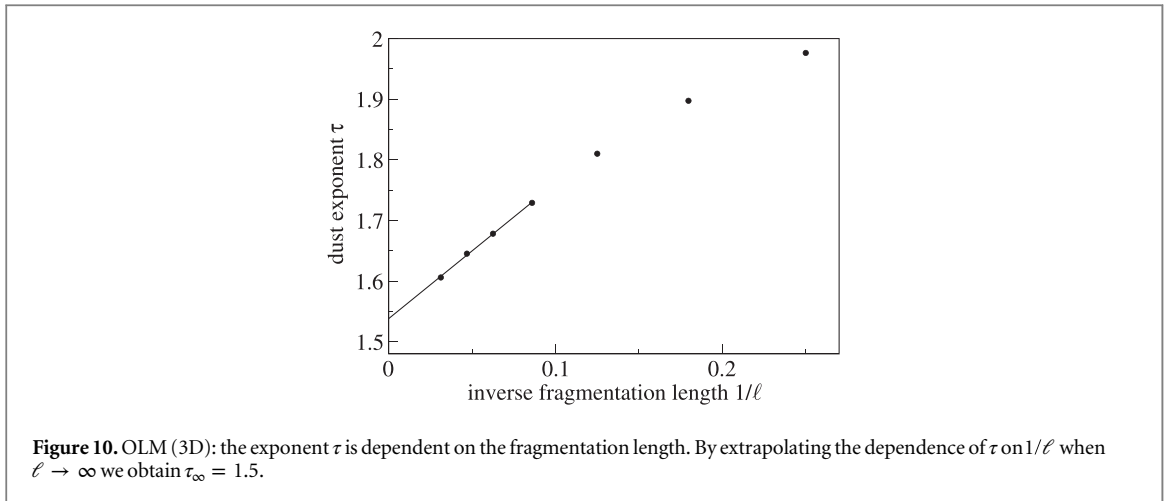


Figure 9. OLM (3D): normalized distribution of fragment masses for various fragmentation lengths. Inset: collapse for $\tau = 1.5$.

$$d_f^{\text{eff}} = 3 + \frac{\Delta \ln (C(r))}{\Delta \ln (r)}, \quad (5)$$

obtained from the local slope. For distances larger than the fragmentation length the structure is effectively no longer fractal, $d_f^{\text{eff}} = 3$. For small values of r the exponents tend to values between 2.2 and 2.4, which is close to the filling height exponent $d_f^{\text{h}} = 2.21$. We do not find a plateau of the local d_f^{eff} values and therefore can, for the system sizes and ℓ values considered, present only an upper bound for d_f^c , which is given in the second column of table 1.

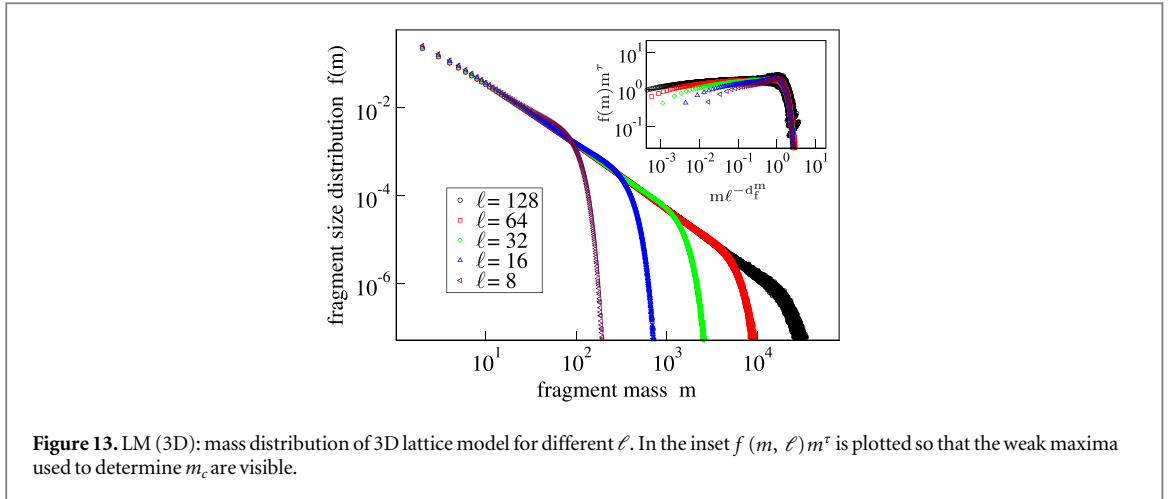
Similarly, for the 3D lattice model of $L = 512$ and $\ell = 128$ one obtains an upper bound of 2.0 for d_f^c (figure 7). In two dimensions the exponent γ can be determined more reliably (figure 8). Nonetheless, it still shows finite size effects. Taking the trends of the effective exponents into account, we get a lower bound of 1.56 for d_f^c . These values are given as d_f^c in table 1.



3.3. Fragment size distribution

The fragment size distribution $f(m, \ell)$ describes the probability density that a fragment has a mass m for fragmentation steps in the steady state. The histogram $f(m, \ell)$ of fragment masses m , normalized to 1, was accumulated over many fragmentation–sedimentation cycles for various fragmentation lengths. Figure 9 shows the results for the 3D OLM. As in two dimensions the fragment mass distribution shows a power law part, composed of ‘dust’ particles by definition, and a peak at the end of the distribution, formed by ‘chunk’ particles with a typical mass m_c . The curves can be well described by a scaling function

$$f(m, \ell) = m_c^{-\tau}(\ell) \tilde{f}\left(\frac{m}{m_c(\ell)}\right), \quad (6)$$



defining the dust exponent τ . It turns out that this exponent, obtained by fitting the power law part of the fragment distribution, varies with the fragmentation length.

Empirically we found that the available data suggest a linear extrapolation in $1/\ell$, which intersects the τ -axis at 1.5 ± 0.1 ; see figure 10. This extrapolated value was used to determine the characteristic chunk mass $m_c(\ell)$ as the maximum of $f(m, \ell)/m^{-\tau}$. The corresponding data collapse of the fragment size distribution function is presented as an inset in figure 9.

We found excellent power law dependence of the characteristic chunk mass on the fragmentation length, figure 11,

$$m_c(\ell) \propto \ell^{d_f^m}. \quad (7)$$

The exponent has the meaning of a fractal dimension of the chunks, $d_f^m = 2.28 \pm 0.03$. It is given in the third column of table 1. We note that the exponent is close to but somewhat larger than the exponent obtained from the dependence of the filling height on the fragmentation length, d_f^h .

We repeated the same analysis of the fragment size distribution function for the lattice model in 2D (figure 12) and 3D (figure 13). The dust exponents are

$$\begin{aligned} \tau(2D) &= 1.377 \pm 0.004 \\ \tau(3D) &= 1.52 \pm 0.03, \end{aligned} \quad (8)$$

The chunks lead to a less pronounced contribution at the end of the distribution than for the off-lattice model. Although they are hardly visible for three dimensions, they are still there, as shown by the inset of figure 13. The fractal exponent of the chunks is

$$\begin{aligned} d_f^m(2D) &= 1.549 \pm 0.007 \\ d_f^m(3D) &= 1.96 \pm 0.03, \end{aligned} \quad (9)$$

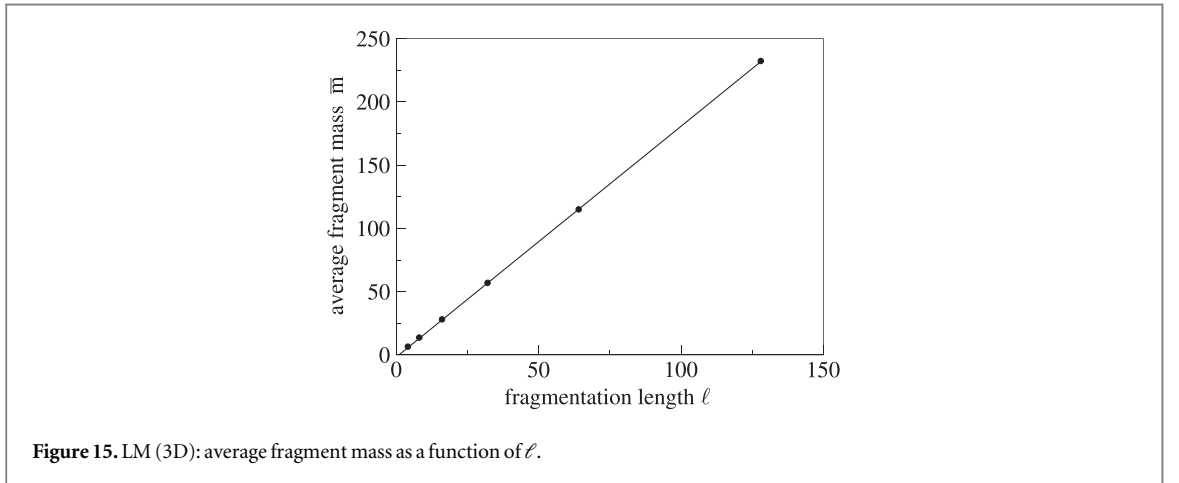
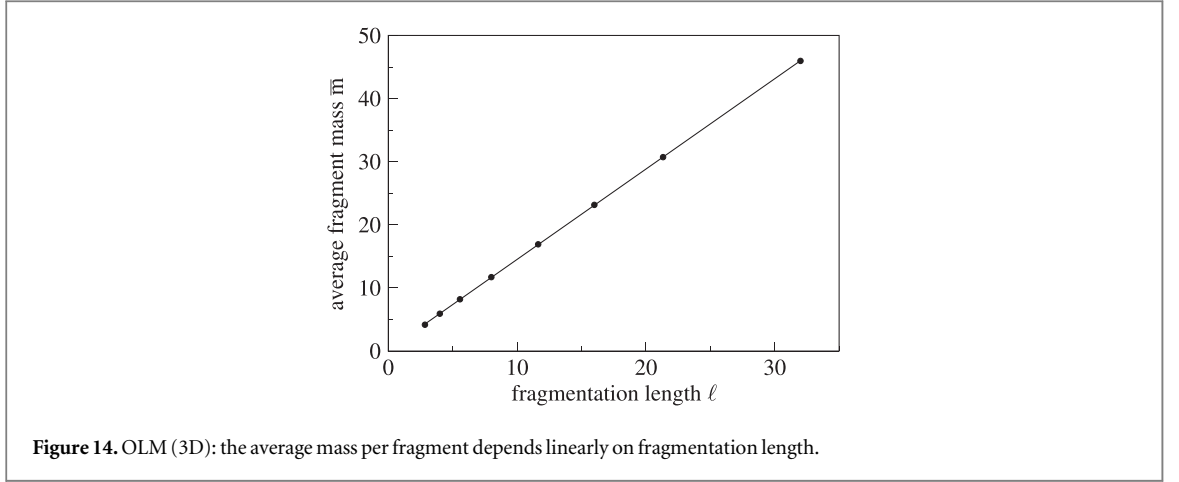
which is 10% smaller than the overall fractal dimension d_f^h , in contrast with the off-lattice case. We conclude that the chunks do not carry the entire mass of one cutout in the limit $\ell \rightarrow \infty$. Further investigations show that not every cutout is populated by a large cluster with characteristic mass m_c . With a nonzero probability, even an empty mesh can be found. In comparison with the OLM, the missing bumps at the end of mass distributions stress this difference as well. This is most certainly caused by the single-contact deposition of clusters. Here one point of contact is enough, which creates more—(i.e., structures that are more porous as opposed to a greater number of porous structures) porous structures because overhangs are not suppressed.

3.4. Scaling relation

In the two-dimensional off-lattice model a scaling relation

$$d_f(2 - \tau) = 1, \quad (10)$$

between the dust exponent and the fractal dimension was derived [2]. Let us briefly go through the arguments here again, this time under the assumption that d_f^h and d_f^m are perhaps different. The argument starts with the observation that the average fragment mass, i.e., the first moment of the distribution function equation (6) is a power law of the chunk mass m_c :



$$\bar{m} = \int_0^{\infty} m f(m, \ell) dm = m_c^{2-\tau} \int_0^{\infty} x \tilde{f}(x) dx. \quad (11)$$

The last integral converges to a constant independent of m_c because \tilde{f} decays faster than any power to zero for $x \gg 1$.

The next step in the argument is the observation that

$$\bar{m} \sim \ell, \quad (12)$$

as demonstrated by figures 14 and 15. This is a consequence of the fact that on average in the steady state as many particle contacts are broken by the fragmentation step as are regained during the sedimentation step. The number of broken contacts around a box cut out in the fragmentation step scales as $\ell^{d_f^h-1}$. Because each fragment upon settlement creates between one and three new contacts depending on the model, the average number n_f of fragments per box must scale the same way,

$$n_f \sim \ell^{d_f^h-1}, \quad (13)$$

Multiplying this by the average fragment mass gives the total mass per box, which according to equation (3) scales as

$$\bar{m} n_f \sim \ell^{d_f^h}. \quad (14)$$

In combination with equation (13) this explains the finding in equation (12).

As a third step the scaling of the chunk mass is inserted in equation (11), which in combination with equation (12) gives

$$\ell \sim \ell^{d_f^m(2-\tau)}. \quad (15)$$

This shows that it should be d_f^m rather than d_f^h that enters the scaling relation in equation (10).

In the last two columns of table 1 it is verified how well the scaling relation is fulfilled with d_f^m (d_f^h). In contrast with the preceding argument, the scaling relation seems to be obeyed by d_f^h better than by d_f^m . We



Figure 16. OLM (2D): sedimentation of needles.

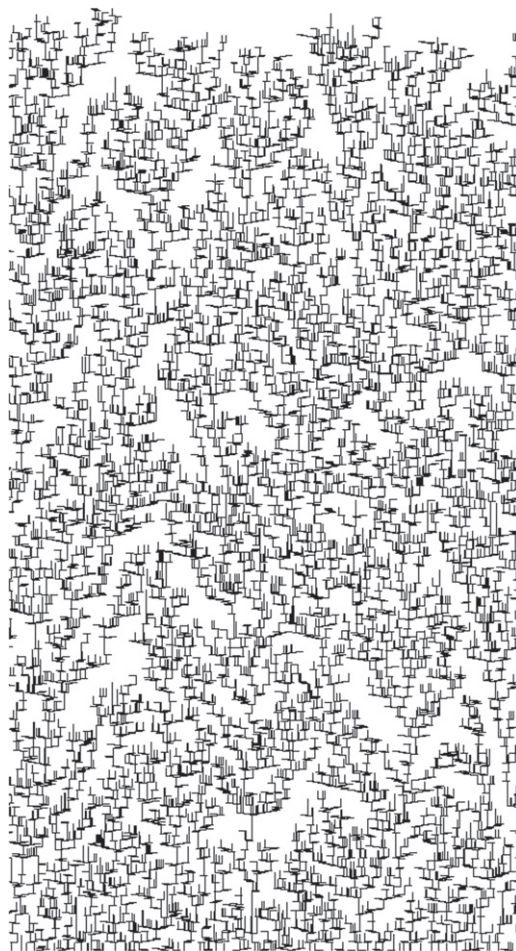
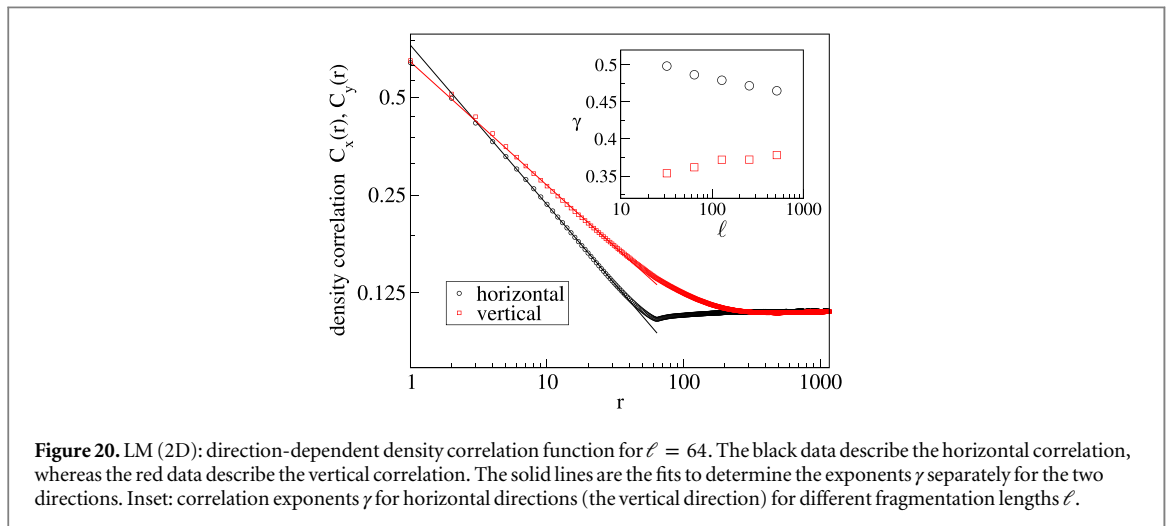
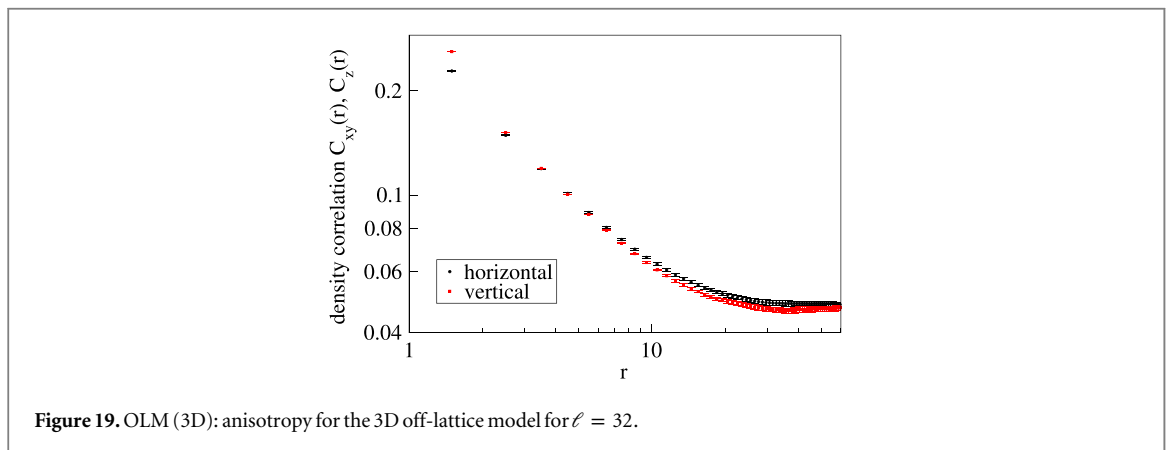
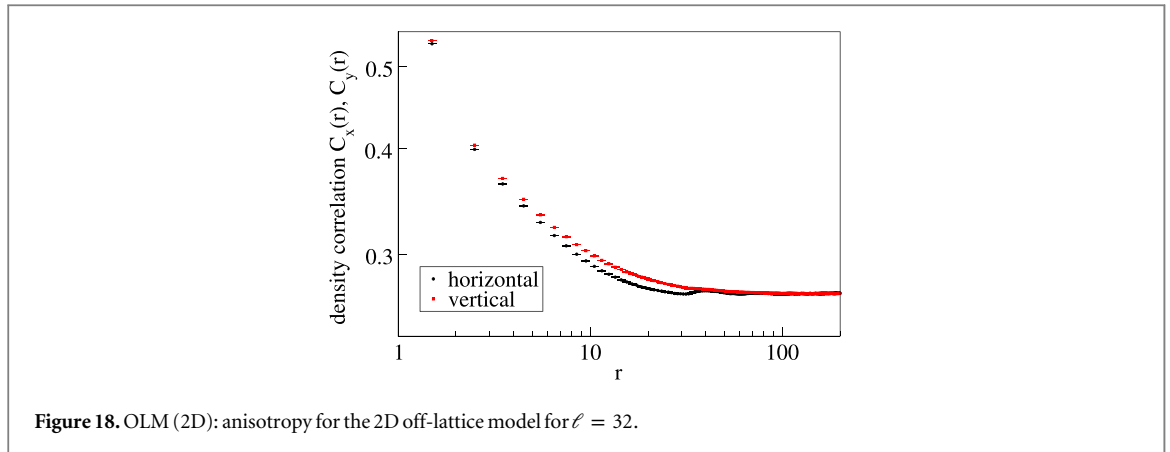


Figure 17. LM (2D): sedimentation of needles.



conclude that the validity of the scaling relation does not give a conclusive criterion regardless of whether the fractal dimension of the chunks is different from that of the boxes cut out by a fragmentation step.

3.5. Anisotropy

Since gravity makes a distinction between the horizontal and the vertical direction, it is of interest to measure whether such a difference exists in the packing. On the one hand, the anisotropy is expected to be weak because it is exclusively due to the last sedimentation process. Any previous anisotropy gets erased by randomly rotating the fragments prior to sedimentation. On the other hand, the example of needles shows that the settlement kinetics may lead to self-organized orientational order, figure 16. In the lattice models such an effect is suppressed because every fragment settles with the random orientation it was prepared in. Still, the example of needles in 2D shows that a horizontal needle in contrast with a vertical one shades the deposit underneath so that

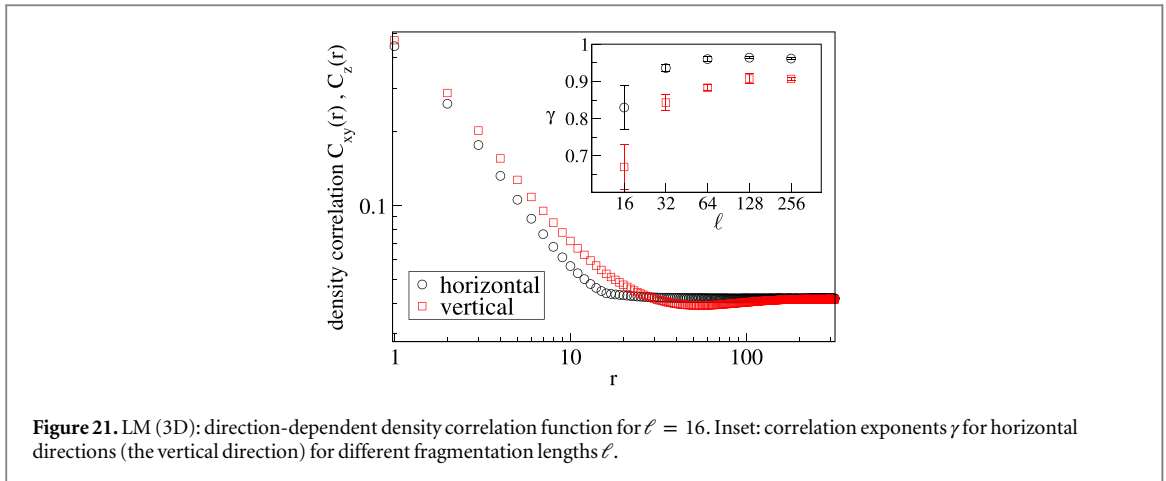


Figure 21. LM (3D): direction-dependent density correlation function for $\ell = 16$. Inset: correlation exponents γ for horizontal directions (the vertical direction) for different fragmentation lengths ℓ .

it is no longer accessible for later needles, figure 17. From this discussion we conclude that anisotropy will develop differently, depending on dimension and settlement kinetics, for the five models considered in this paper.

Here we analyze only the effect of anisotropy on the density correlation function, equation (4), because of its connection to the fractal dimension. For this purpose, \vec{r} is either in the vertical direction, giving the vertical correlation function, or in horizontal directions, giving the horizontal correlation function, which was averaged over all horizontal directions. Asymptotically, the density correlation always becomes equal to the density, i.e., independent of direction.

The measured functions are displayed in figures 18 and 19 for the two-dimensional and three-dimensional off-lattice models respectively, averaged in the bulk of the system with $L = 128$ and $N = 5 \times 10^6$. As expected, the anisotropy is visible in the density correlation function only up to a distance of order ℓ . It is more pronounced in the two-dimensional case. In the three-dimensional case, the difference between the functions is small: the density correlation for the vertical direction decays a little faster than for horizontal directions.

Figures 20 and 21 show the direction-dependent density correlation function for the lattice model in two and three dimensions respectively. Here, in contrast with the off-lattice model, the decay in horizontal directions is faster, reflecting the different microscopic origin of the anisotropy. The inset of figure 20 shows the exponents γ for different ℓ . The difference between the horizontal directions and the vertical direction decreases with increasing ℓ , implying that it perhaps even vanishes in the limit $\ell \rightarrow \infty$.

A tangible proof that for very large ℓ we are dealing with an isotropic system has yet to come. Hence we can conclude that anisotropy causes a systematic error in quantities measured by varying ℓ .

4. Conclusions

We have studied the structure of a 3D nanopowder subjected to repeated fragmentation and sedimentation, and compared it with results for a 2D nanopowder. The fragmentation was simulated by disassembling the packing with a cubic mesh, whereas for the sedimentation two different models were developed. In the more realistic one the complex-shaped fragments were dropped with orientation and horizontal position chosen randomly, followed by a steepest-descent relaxation. In the computationally more efficient lattice model, on the other hand, this relaxation was suppressed: the fragments stuck upon first vertical contact in the orientation they were prepared in.

We found that the qualitative behavior in 3D is similar to the 2D nanopowder:

- (i) After a relaxation time linear in the fragmentation length ℓ , a stationary structure is reached.
- (ii) The asymptotic filling height depends as a power law on the fragmentation length, indicating a fractal substructure with a fractal dimension d_f^h .
- (iii) The density correlation analysis confirmed that the effective fractal dimension is smaller than 3 for distances shorter than the fragmentation length, and equal to 3 for larger distances.
- (iv) The fragment size distribution is composed of a power law part (dust) and a bump at the end of the distribution (chunks).

- (v) The fragment size distribution can be described by a scaling function with two exponents, the dust exponent τ and the fractal dimension of the chunks d_f^m .

The exponents are summarized in table 1. A few interesting observations can be made: first, the 3D lattice model and the 3D off-lattice model without relaxation give very consistent exponents. This shows that the discretization of the fragment rotation in the lattice model is not relevant to the scaling behavior. Second, for the lattice models in 2D and in 3D the fractal dimension of the chunks, d_f^m , seems to be smaller by about 10% than for the corresponding off-lattice models with relaxation. A possible explanation for this is that relaxation makes the sediment denser, hence leading to a larger effective dimension. The question of whether this difference survives in the scaling limit $\ell \rightarrow \infty$ is very difficult to answer, though. A hint can be obtained by comparing d_f^m with d_f^h for the lattice models, the former being 3% (2D) and 8% (3D) smaller. Therefore, the scaling relation $d_f(2 - \tau) = 1$, which, according to its theoretical derivation, should hold for $d_f = d_f^m$, should be violated for d_f^h . However, the opposite is true (see the last two columns in table 1). This can be taken as an indication that the fractal dimensions will actually be the same in the scaling limit.

In conclusion, we found that the fractal dimension for a 3D nanopowder subjected to repeated fragmentation and sedimentation is 2.1 ± 0.1 (compared with 1.6 ± 0.1 for 2D). The dust exponent τ obeys the scaling relation $d_f(2 - \tau) = 1$. We showed that these exponents are not changed by relaxation, nor by the different mechanisms creating anisotropies in the models.

We suggest two directions for further research. The model has several simplifications, in particular concerning the fragmentation process, and therefore more realistic simulations are of interest. Finally, experimental realizations are needed to validate the results.

Acknowledgments

We thank the German Science Foundation (DFG) for funding through the Cluster of Excellence ‘Engineering of Advanced Materials’, grants WO 577/9-1 and PO472-22-1 and Collaborative Research Center SFB814. We acknowledge support by Deutsche Forschungsgemeinschaft and Friedrich-Alexander-Universität Erlangen-Nürnberg within the funding program Open Access Publishing.

References

- [1] Mädler L, Lall A A and Friedlander S K 2006 *Nanotechnology* **17** 4783
- [2] Schwager T, Wolf D E and Pöschel T 2008 *Phys. Rev. Lett.* **100** 218002
- [3] Visscher W M and Bolsterli M 1972 *Nature* **239** 504
- [4] Pöschel T and Schwager T 2005 *Computational Granular Dynamics: Models and Algorithms* (Berlin: Springer)
- [5] Bratberg I, Radjai F and Hansen A 2002 *Phys. Rev. E* **66** 031303
- [6] Voivret C, Radjai F, Delenne J Y and el Youssoufi M S 2007 *Phys. Rev. E* **76** 021301
- [7] Jullien R and Meakin P 1987 *Europhys. Lett.* **4** 1385
- [8] Jullien R and Meakin P 1990 *Nature* **344** 425
- [9] Jullien R, Meakin P and Pavlovitch A 1992 *Phys. Rev. Lett.* **69** 640
- [10] Schwartz L M, Wilkinson D J, Bolsterli M and Hammond P 1993 *Phys. Rev. B* **47** 4953
- [11] Baumann G, Jobs E and Wolf D E 1993 *Fractals* **1** 767
- [12] Baumann G, János I M and Wolf D E 1994 *Europhys. Lett.* **27** 203
- [13] Baumann G, János I M and Wolf D E 1995 *Phys. Rev. E* **51** 1879
- [14] Baumann G and Wolf D E 1996 *Phys. Rev. E* **54** R4504
- [15] Topic N, Gallas J A C and Pöschel T 2012 *Phys. Rev. Lett.* **109** 128001
- [16] Topic N, Gallas J A C and Pöschel T 2013 *Phil. Mag.* **93** 4090
- [17] Carmona H A, Wittel F K and Kun F 2014 *Eur. Phys. J. Spec. Top.* **223** 2369
- [18] Martín M A, Muñoz F J, Reyes M and Taguas F J 2014 *Pure. Appl. Geophys.* **1–8**
- [19] Schwager T and Pöschel T 2006 Efficient numerical simulation of granular matter using the bottom-to-top reconstruction method *Behavior of Granular Media* ed P Walzel, S J Linz, C A Kruelle and R Grochowski (Aachen: Shaker) p 151
- [20] Wolf D E, Pöschel T, Schwager T, Weuster A and Brendel L 2009 *AIP Conf. Proc.* **1145** p 859
- [21] Hoshen J and Kopelman R 1976 *Phys. Rev. B* **14** 3438
- [22] Caglioti E, Loreto V, Herrmann H and Nicodemi M 1997 *Phys. Rev. Lett.* **79** 1575
- [23] Meakin P, Ramanlal P, Sander L M and Ball R C 1986 *Phys. Rev. A* **34** 5091
- [24] Witten T A and Sander L M 1981 *Phys. Rev. Lett.* **47** 1400